

Structure beneath the Alboran from geodynamic flow models and seismic anisotropy

Lisa A. Alpert,^{1,2} Meghan S. Miller,¹ Thorsten W. Becker,¹ and Amir A. Allam¹

Received 24 January 2013; revised 21 July 2013; accepted 27 July 2013; published 16 August 2013.

[1] Upper mantle heterogeneity beneath the Alboran Sea (western Mediterranean) as inferred from seismology has been associated with a range of subduction and lithospheric delamination scenarios. However, better constraints on the deep dynamics of the region are needed to determine the cause and consequence of complex surface tectonics. Here, we use an improved set of shear wave splitting observations and a suite of mantle flow models to test a range of suggested structures. We find that the observed seismic anisotropy is best reproduced by mantle flow models that include a continuous, deeply extending slab beneath the Alboran which elongates along the Iberian margin from Granada to Gibraltar and curves southward toward the High Atlas. Other models with detached slabs, slabs with spatial gaps, or drip-like features produce results inconsistent with the splitting observations. SW-directed shear flow, when combined with sublithospheric deflection in response to a dense sinker, generates NNW-splitting orientations most similar to the patterns observed along Gibraltar. Slab viscosities of ~ 250 times that of the upper mantle are preferred because they provide a balance between the poloidal flow induced by any sinker and toroidal flow induced by stiff slabs. The best match to anisotropy across the Atlas is a model with a stiff continental keel in northwestern Africa which deflects flow northward. Our results show that quantitative predictions of seismic anisotropy are useful in distinguishing the spatial and depth extent of regional density structures which may otherwise be ambiguous.

Citation: Alpert, L. A., M. S. Miller, T. W. Becker, and A. A. Allam (2013), Structure beneath the Alboran from geodynamic flow models and seismic anisotropy, *J. Geophys. Res. Solid Earth*, 118, 4265–4277, doi:10.1002/jgrb.50309.

1. Introduction

[2] The Alboran domain sits between Spain and Morocco and marks the westernmost terminus of what used to be the Tethyan subduction belt between the slowly converging African and Eurasian plates. This greater Alboran system includes the Gibraltar structural arc, which is made up of the Betic mountains in Spain and the Rif mountains of Morocco, which wrap around the Alboran Sea, and the Atlas mountains several hundred kilometers to the south (Figure 1a). One of the strong pieces of evidence for subduction beneath the Alboran is the presence of reoccurring deep (> 600 km) seismicity beneath Granada, the most recent of which occurred in April 2010 [e.g., Gutscher *et al.*, 2002; Buforn *et al.*, 2011; Bezada and Humphreys, 2012], yet only a small amount of oceanic lithosphere is observed in the western Mediterranean. This makes typical subduction scenarios ambiguous, and the Cenozoic tectonics are cor-

respondingly complex. As a consequence, there have been several hypotheses to explain the regional tectonics and variety of geophysical observations, which cover lithospheric delamination [e.g., Platt and Vissers, 1989; Seber *et al.*, 1996; Zeck, 1996; Jiménez-Munt *et al.*, 2011], various styles of subduction [e.g., Blanco and Spakman, 1993; Royden, 1993; Faccenna *et al.*, 2004; Diaz *et al.*, 2010], lithospheric drips [e.g., Bokelmann and Mauffro, 2007], and a buoyant mantle upwelling and lithospheric thinning across Morocco to explain the topography, geochemistry, and potential field observations [e.g., Anguita and Hernán, 2000; Duggen *et al.*, 2009]. Current debate is focused on the direction and evolution of subduction of at least some portions of an otherwise detached slab beneath the Gibraltar arc in conjunction with slab rollback, suggested, for example, by Jolivet *et al.* [2009], Pedrera *et al.* [2011], Gutscher *et al.* [2012], and Bezada *et al.* [2013] and questioned by Platt *et al.* [2013].

[3] What is clear is that the Alboran system is shaped by complex interactions between the lithosphere and mantle. Distinguishing between suggested mantle-based drivers for the tectonics has been further complicated by incomplete seismic data coverage. Here, we make use of existing and newly available seismic anisotropy observations in the region and use quantitative models of mantle flow to distinguish between likely and unlikely mantle structure. We calculate the predicted anisotropy based upon shear wave

¹Department of Earth Sciences, University of Southern California, Los Angeles, California, USA.

²Now at Aera Energy LLC, Bakersfield, California, USA.

Corresponding author: M. S. Miller, Department of Earth Sciences, University of Southern California, 3651 Trousdale Pkwy., Los Angeles, CA 90089, USA. (msmiller@usc.edu)

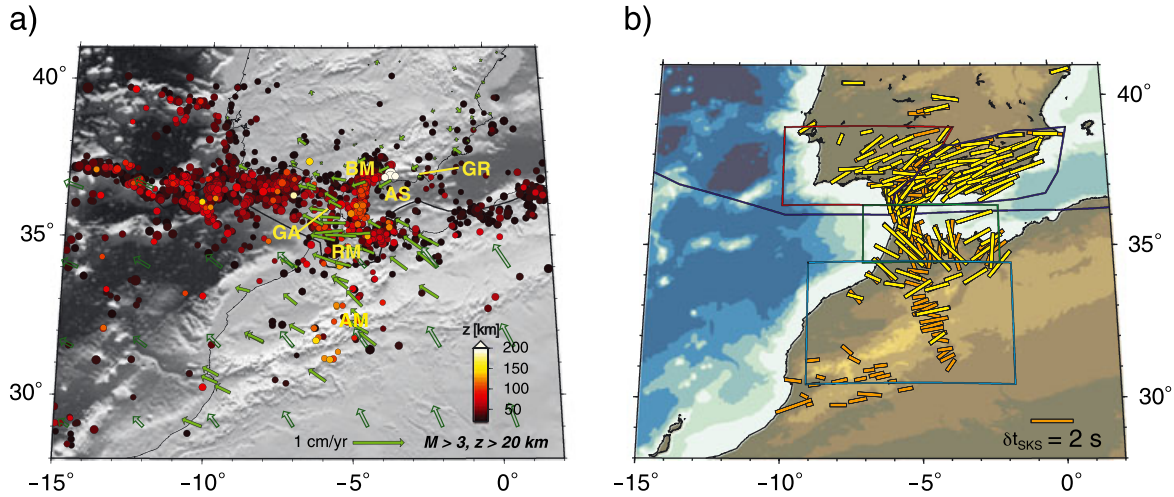


Figure 1. (a) Tectonic setting of the Alboran region, western Mediterranean. Seismicity is shown color coded by depth for events deeper than 20 km (ING Spain catalog, 1960 to 10/2012, magnitude $M \geq 4$) on top of shaded topography with plate boundary geometry from *Bird* [2003] as a black line. Green crustal velocity vectors are shown in a Eurasia-fixed reference frame from the long-term plate motion model NUVEL-1A (open vectors) [DeMets *et al.*, 1994] and from geodetic estimates by *Koulali et al.* [2011]. GR: Granada, BM: Betic Mountains, AM: Atlas Mountains, GA: Gibraltar arc, RM: Rif Mountains, and AS: Alboran Sea. (b) Station-averaged SKS splitting (fast polarization orientation and delay time indicated by stick azimuth and length, respectively) plotted centered at station location from the *Wüstefeld et al.* [2009] compilation (as of 12/2012) which includes the studies of *Buontempo et al.* [2008] and *Diaz et al.* [2010] (yellow), and new results from recent deployments (orange) [Miller *et al.*, 2013]. Polygons indicate regional subsets considered in the discussion and Table 2 with red and blue for “Spain W” and “Spain E,” green for “Gibraltar,” and cyan for the “Atlas” domains.

splitting and present the first quantitative forward model of anisotropy for the region. Such modeling provides new insights into the interactions between mantle dynamics and lithospheric deformation.

[4] We compute models of instantaneous, global mantle flow from which we calculate elastic anisotropy and synthetic shear wave splitting using the approach of *Becker et al.* [2006a, 2006b]. Such model predictions are regionally very sensitive to the position and morphology of upper mantle density anomalies; therefore, we test a range of density models. The assorted tectonic models proposed for the region are based on geophysical observations, such as differently oriented slab- and drip-like structures extending to various depths, which are investigated in our computations. We compare the predicted anisotropy for this suite of models with splitting observations from the *Wüstefeld et al.* [2009] compilation (as of 12/2012, which in the study region consists mainly of measurements from *Buontempo et al.* [2008] and *Diaz et al.* [2010]) and our own analysis of new data (Figure 1b) [Miller *et al.*, 2013]. This enables us to investigate the plausible range of mantle density and viscosity structures and its influence on mantle flow and regional tectonics.

2. Shear Wave Splitting Observations

[5] Seismic anisotropy in the upper mantle is typically attributed to the lattice preferred orientation (LPO) of intrinsically anisotropic upper mantle minerals, mainly olivine [e.g., *Silver*, 1996]. The link between the formation of LPO and progressive deformation of mantle rocks [e.g.,

Ben Ismail and Mainprice, 1998; *Karato et al.*, 2008] can then be used to make inferences on mantle flow from observations of anisotropy [e.g., *Tanimoto and Anderson*, 1984; *Long and Becker*, 2010]. One of the most direct observations of anisotropy comes from shear wave splitting [e.g., *Vinnik et al.*, 1989; *Savage*, 1999]. Shear waves traveling through an anisotropic material will split into two orthogonally polarized waves, one propagating in the fast velocity polarization plane (the “fast axis”) and one in the slow orthogonal plane. A shear wave splitting measurement consists of the delay in arrival time between the fast and slow shear waves recorded at a seismic station and the inferred fast polarization orientation.

[6] Assuming the origin of the observed seismic anisotropy is from LPO formed under mantle flow allows for exploration of geodynamic scenarios [e.g., *Silver*, 1996; *Long and Becker*, 2010]. Previous shear wave splitting investigations for the western Mediterranean found that apparent fast polarization orientations produce a pattern similar to that of the Gibraltar arc curvature [Buontempo *et al.*, 2008; *Diaz et al.*, 2010] (Figure 1b), which was associated

Table 1. Model Parameters^a

Variable Name	Symbol	Value
Reference viscosity	η_0	10^{21} Pa s
Rayleigh number		$3.4 \cdot 10^8$
Reference density	ρ_0	3500 kg m ⁻³
Slab/upper mantle density contrast	$\Delta\rho$	3.9%

^aThe Rayleigh number is defined using the Earth’s radius as in *Zhong et al.* [2000].

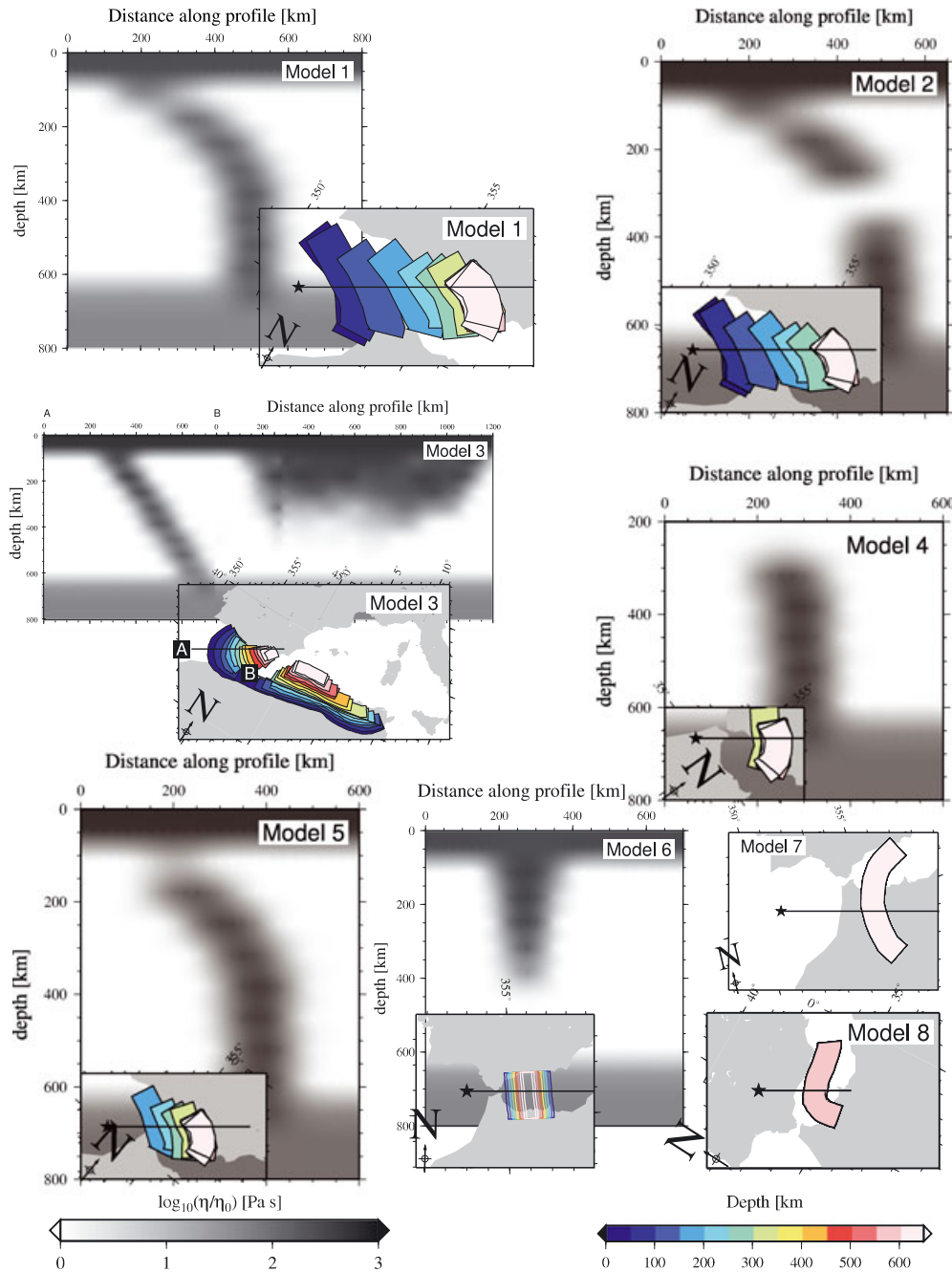


Figure 2. Figures showing slab morphology and depth extent of selected density models (1 through 8) tested. Gray scale shading is viscosity and colored shading is depth of the contours for the tested structure. Inset map shows location and orientation of the anomaly. For models 7 and 8, as described in the text, the slabs are vertical from 100 to 650 km depth.

with trench rollback and escape flow around the slab by *Diaz et al.* [2010]. New measurements that stretch between Iberia and southern Morocco consist of ~ 1300 individual, teleseismic *SKS* splitting observations from the recent PICASSO experiment and contemporaneous deployments (Figure 1b) [Miller et al., 2012].

[7] The splitting measurements in all of the main studies for the region [Buontempo et al., 2008; Diaz et al., 2010; Miller et al., 2012] were conducted using the Matlab software package Splitlab [Wüstefeld et al., 2008], ensuring a

degree of methodological consistency. Our new results in Figure 1b are derived using the rotation-correlation method of *Bowman and Ando* [1987], which aims to find the optimum fast axis (azimuth), α , and delay time, δt , such that horizontal particle motion is linearized when the delayed phase has been corrected, advanced in time by δt and rotated by α . Details of the new analysis of teleseismic *SKS* and local *S* shear wave splitting are given by *Miller et al.* [2013]. Here, we focus on station-averaged splits (see, e.g., discussion in *Becker et al.* [2006b]), on the degree of depth-resolution that

Table 2. Regional Seismic Anisotropy Misfits According to Subsets of Data as Sorted by the Polygons Shown in Figure 1b, Evaluated for the Example Geodynamic Model Predictions as Considered in Figures 4–7^a

Model Type	Region Name							
	Spain W		Spain E		Gibraltar		Atlas	
	$\langle\Delta\alpha\rangle$	$\langle\Delta(\delta t)\rangle$						
NE, ref.	26.8	0.49	27.6	0.11	46.7	0.12	45.1	0.62
SW, ref.	24.3	0.01	16.8	-0.34	50.1	-0.48	54.5	0.12
NE, model 1	59.9	-0.15	47.4	-0.79	45.0	0.05	46.9	0.40
SW, model 1	64.8	0.03	47.3	-0.57	41.2	-0.28	65.4	0.32
NE, model 8	62.8	0.58	65.6	-0.31	59.4	-0.57	51.7	0.54
SW, density model 8	67.4	0.69	65.4	-0.14	46.8	-0.89	73.3	0.45
NE, model 8, stiff slab	32.5	-0.15	47.2	-0.59	44.8	-0.36	43.6	0.40
SW, model 8, stiff slab	25.4	-0.02	29.8	-0.27	31.0	-0.55	33.0	-0.08
NE, model 8, stiff slab & keel	24.0	0.19	37.0	-0.39	62.8	-0.40	60.4	-0.27
SW, model 8, stiff slab & keel	22.8	0.02	22.8	-0.19	30.4	-0.56	15.7	-0.28

^aRef is the reference flow model and the average, angular misfit for apparent “fast axes,” $\langle\Delta\alpha\rangle$, is given in degrees and average delay time misfit, $\langle\Delta(\delta t)\rangle$, is in seconds. “NE” and “SW” refer to NE and SW flow type models, respectively.

back-azimuthal information can provide). This leads to 199 sites with measurements which are used for modeling and shown in Figure 1b. Here, we use a prior version of the SKS splitting data set from *Miller et al.* [2012], but employing the final version as of *Miller et al.* [2013] would lead to insignificant differences in the quantitative misfit metrics ($< 0.5^\circ$ for angular misfits), and visually indistinguishable results.

[8] The improved set of splitting observations for the region shows a predominant ENE orientation of fast axes along the Betics in southern Spain and within the Alboran Sea, with rotation to the NNW along Gibraltar [*Diaz et al.*, 2010; *Miller et al.*, 2013], and little correspondence to a simple mantle shear scenario that may be inferred from plate motions (Figure 1a). In northeastern Morocco, the NNW orientations continue southward until the High Atlas mountains, where they rotate E-W, and delay times decrease in amplitude. We explore which geodynamic models are capable of capturing these features to first order, in order to investigate mantle structure and resulting mantle flow patterns.

3. Modeling Methods

3.1. Global Mantle Flow

[9] To model mantle circulation, we use CitcomS [*Zhong et al.*, 2000], a spherical finite element code based on Citcom [*Moresi and Gurnis*, 1996], from the Computational Infrastructure for Geodynamics (geodynamics.org). The flow modeling procedure is described in detail in *Alpert et al.* [2010]. Here, we briefly discuss the incorporation of lateral viscosity variations and temperature anomalies adjusted for the Alboran domain. Our computations are performed at a horizontal numerical resolution of ~ 25 km by ~ 22 km from the surface to the core-mantle boundary, ensuring that regional tectonics can be explored in global circulation framework [cf. *Faccenna and Becker*, 2010; *Becker and Faccenna*, 2011].

[10] Density anomalies in the mantle circulation model are incorporated from the regionalized upper mantle (RUM) model of *Gudmundsson and Sambridge* [1998]. RUM slabs are contours of seismicity based on the *Engdahl et al.* [1998] earthquake catalog, and those are converted to polygons corresponding to 100 km thick slabs and interpolated at 50 km

depth intervals. Within each polygon, a constant temperature of zero is assigned compared to the background mantle of nondimensional temperature unity. The strength of this thermal anomaly is then controlled by the Rayleigh number, and we chose the scaling such that slabs have a uniform density anomaly of 3.9% (Table 1).

[11] The lithosphere is defined as the outermost layer of the model that extends between the surface and 100 km depth and is modeled as a fluid with viscosities (η_{lith}) of η_0 , $50\eta_0$, $250\eta_0$, and $500\eta_0$, where η_0 is the upper mantle reference viscosity (Table 2). Below the lithosphere, the slab viscosity (η_{slab}) is controlled with a temperature-dependent rheology $\eta = \eta_0 \exp(E(\Delta T))$, where E determines the strength of the temperature dependence and ΔT is the temperature difference between the slab and the ambient mantle. Given our choices for the temperature structure of slab and mantle, the maximum slab viscosity is $\eta_0 \exp(E)$. Values for E were chosen to most closely match the lithosphere viscosity which is controlled by a preexponential factor applied to the lithospheric layer. The lower mantle extends from 660 km to 2891 km and is modeled with a viscosity increase of $50\eta_0$. The effect of the craton in northwestern Africa is tested by assigning a $100\eta_0$ viscosity to the cratonic regions as defined in the 3SMAC model of *Nataf and Ricard* [1996] down to 300 km. Although inconsistent with LPO development by dislocation creep, all of our models are Newtonian. We consider this and our assumption of temporally constant mantle flow as reasonable simplifications, characteristic of mantle flow for the last few Myr [*Becker et al.*, 2003; *Becker*, 2006]. From these reference models, we vary the mechanical surface boundary conditions, density models, and viscosity parameters as described next.

3.1.1. Mechanical Boundary Conditions and Two Different Modes of Large-scale Mantle Shear

[12] Surface boundary conditions are prescribed by the NUVEL-1A (Figure 1a) [*DeMets et al.*, 1994] plate motions, either in the no-net rotation reference frame or the HS3 absolute plate motion model of *Gripp and Gordon* [2002]. For no-net rotation reference frame models, we use a free-slip boundary condition at the core-mantle boundary (CMB). For HS3 reference frame models, a no-slip CMB boundary condition is used to induce net rotation related shearing

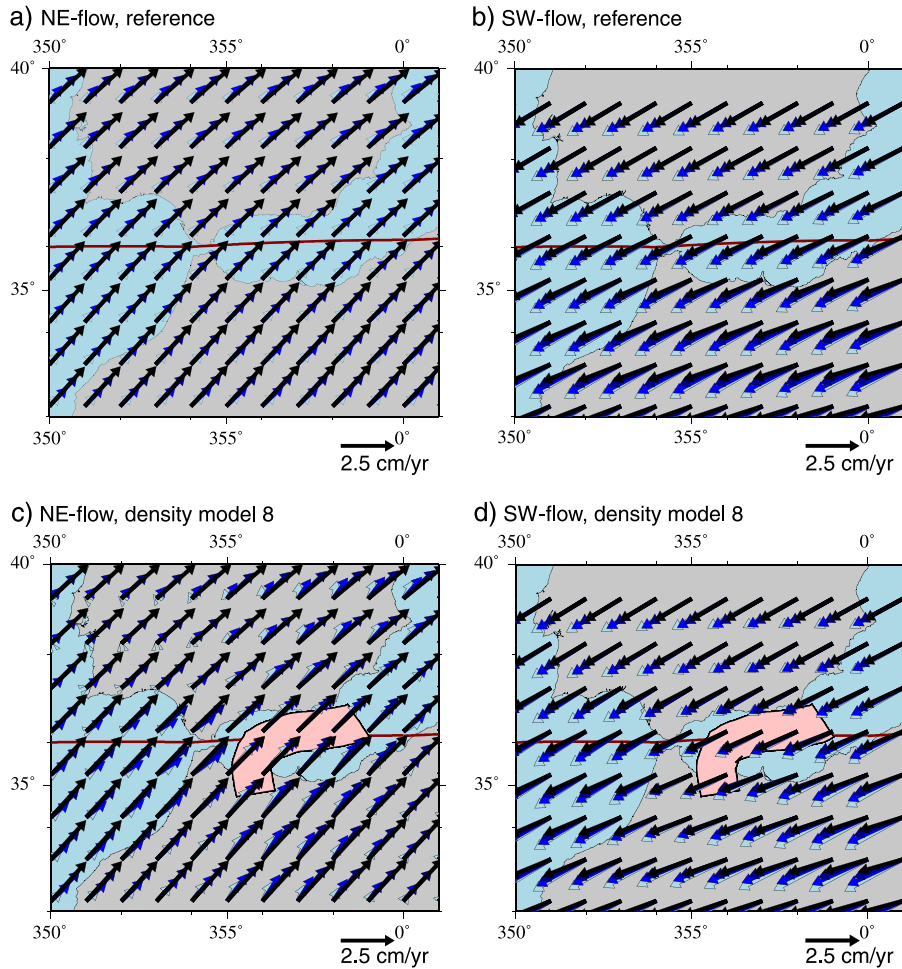


Figure 3. Depth dependence of mantle flow for different kinematic boundary conditions ((a, c) NE and (b, d) SW flow models) with reference flow model (Figures 3a and 3b, cf. Figure 4 for anisotropy) and additional density model 8 (Figures 3c and 3d, cf. Figure 6), with slab viscosity of $\eta_{\text{slab}} = 250$. Depths of 0, 150, 250, and 350 km shown, dark to bright colors. Note how flow maintains the plate motion orientation with depth for NE flow models while SW flow models show a response to the induced shear due to net rotation. With the addition of a buoyancy anomaly in the Alboran Sea (cf. Figure 2), note how NE flow responds to the anomaly most strongly in the northeast of the domain while the response for SW flow is strongest near Gibraltar and to the southwest.

[cf. *Conrad and Behn, 2010*]. Fixing the CMB and prescribing absolute plate motion, we find that the models with net rotation channel the associated shear flow into the upper mantle, similar to what is observed in consistently generated net rotation models [e.g., *Zhong, 2001; Becker, 2006*]. We use these end-member surface boundary conditions to generate opposite sense plate-related shear flow in the region, NE for no-net rotation and SW for HS3, without a necessary inference to a preferred reference frame [cf. *Dogliani et al., 2007; Becker, 2008; Kreemer, 2009; Conrad and Behn, 2010*]. In this paper, we distinguish the surface plate motion reference frames as NE and SW flow models in order to highlight the effect of the mantle shearing, as opposed to its origin, which is not entirely clear.

3.1.2. Additional Density Models

[13] We investigate suggestions for possible upper mantle structure beneath the Alboran Sea not captured by the reference model, by incorporating various density structures,

representing suggested slab or lithospheric delamination scenarios, into the reference model based on RUM. We explore 21 scenarios for this purpose but present in Figure 2 eight models that reflect the most characteristic and interesting results. Model 1 includes a NE-dipping slab extending from the surface along the Gibraltar arc to 650 km, which is based upon structure inferred by *Lonergan and White [1997], Gutscher et al. [2002], and Diaz et al. [2010]*. Model 2 has a NE-dipping slab as in model 1, but with a gap from 300 to 400 km, motivated by the *P* wave tomography of *Li et al. [2008]*. Model 3 includes two separate pieces of slab material, a N-dipping slab along the northern African margin and a NE-dipping slab beneath the Gibraltar Arc, both extending from 100 to 650 km, and separated from each other by two slab windows as suggested by *Faccenna et al. [2004]*. Model 4 has a slab structure that dips to the NE between 300 to 650 km but is detached from the surface beneath the Alboran Sea, as inferred from *Platt*

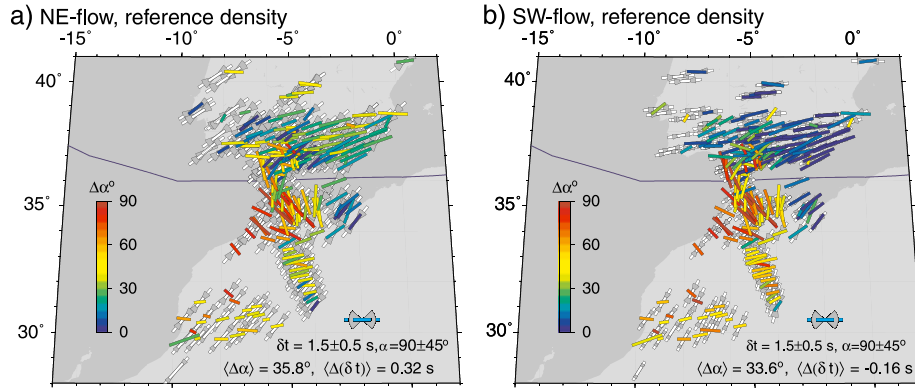


Figure 4. Effect of mantle shear on seismic anisotropy prediction. Figures show shear wave splitting for the reference viscosity and density model (no additional, regional anomalies) for (a) NE and (b) SW flow models; radial viscosity variations only. Average fast polarization orientations, α , are shown with white bars, scaled by delay time (δt), including splitting variations as a function of back azimuth (gray). Legend symbol with cyan sticks indicates arbitrary prediction of $\delta t = 1.5 \pm 0.5$ s and $\alpha = 90 \pm 45^\circ$ for scale. Actual splitting observations are shown colored by the local angular misfit ($\Delta\alpha$). Radial viscosity structure is $\eta_{\text{lith}} = 50$ and $\eta_{\text{lm}} = 50$. The number of splitting observations (station averaged) is 199, and the regional averaged, mean angular, $\langle\Delta\alpha\rangle$, and delay time, $\langle\Delta(\delta t)\rangle$, misfits for the model are given in the legend. Table 2 lists regional misfits for this and the other example model results as defined in Figure 1b. The dark blue line is the NUVEL-1A [DeMets *et al.*, 1994] plate boundary.

and Vissers [1989], Seber *et al.* [1996], and Zeck [1996]. Model 5 has a similar structure as in model 4, but with a gap in the slab structure extending between 150 and 650 km similar to the model proposed by Blanco and Spakman [1993]. Model 6 includes a structure representing a symmetric “drip” east of the surface expression of the Gibraltar arc extending from the surface down to 400 km as in Bokelmann and Mauffro [2007]. Model 7 includes a vertically dipping slab that is concave to the SE and centered directly east of the Gibraltar Arc and extending into the High Atlas based upon results by Bijwaard *et al.* [1998]. The last model, 8, includes a slab structure along the Iberian margin curving southward around the Gibraltar Arc, similar to what was imaged by Spakman and Wortel [2004], but mainly guided by trial and error adjustments during an iterative fitting procedure of the seismic anisotropy observations.

3.2. Modeling Seismic Anisotropy Based on Mantle Flow

[14] We assume that upper mantle anisotropy is mainly caused by LPO alignment of intrinsically anisotropic olivine by mantle flow in the dislocation creep regime. Consequentially, LPO may be expected to form within the upper ~ 400 km of the mantle [e.g., Karato, 1992; Fischer and Wiens, 1996; Becker, 2006], affecting seismic waves in our models by traversing the depth range between ~ 50 km and ~ 350 km. Evidence for the alignment of crystallographic axes of anisotropic minerals with the direction of shear in laboratory experiments [e.g., Karato *et al.*, 2008] combined with petrological observations [e.g., Ben Ismail and Mainprice, 1998] have led to quantitative models of LPO development [e.g., Wenk and Tomé, 1999; Tommasi *et al.*, 2000; Kaminski and Ribe, 2001]. Such techniques provide a link between geodynamic and seismic models. Our approach is motivated by the successful modeling of observed upper mantle anisotropy in regional [e.g., Fouch *et al.*, 2000; Hall *et al.*, 2000; Blackman and Kendall, 2002; Gaboret *et al.*, 2003; Behn

et al., 2004; Becker *et al.*, 2006b; Miller and Becker, 2012] and global applications [e.g., Becker *et al.*, 2003, 2008; Conrad and Behn, 2010].

[15] As in Becker *et al.* [2006b], we follow the kinematic approach of Kaminski and Ribe [2001] to model the development of LPO in response to convective flow in the mantle. We use the D-REX program and parameter choices for regular (“A type”) olivine LPO with coaligned enstatite from Kaminski *et al.* [2004] to calculate the resultant seismic anisotropy predicted from our circulation model by computing velocity gradient tensors along particle paths, assuming steady state flow. Tracers are advected in mantle flow, developing LPO along the flow path until the logarithmic finite strain, ξ , reaches a critical value of ξ_c , which is set at 0.5. Larger values will mainly affect LPO saturation and hence anisotropy amplitudes and delay times, rather than azimuths [Becker *et al.*, 2006b; Miller and Becker, 2012]. Then a Voigt-averaged elasticity tensor is computed for each location of interest, and we use the full elasticity tensor to compute synthetic waveforms using a propagator matrix approach. From those, shear wave splitting is computed using an automated rotation-correlation method (for details, see Becker *et al.* [2006b]).

[16] To evaluate model performance quantitatively, we compare the observed and synthetic splitting measurements and compute the absolute, angular deviation of apparent fast orientation azimuths or “fast azimuths,” $\Delta\alpha$ ($0 \leq \Delta\alpha \leq 90^\circ$, where an average misfit of $\langle\Delta\alpha\rangle = 45^\circ$ is expected for random distributions), and the delay time misfit $\Delta\delta = \delta t_{\text{model}} - \delta t_{\text{data}}$ ($\Delta\delta > 0$ indicates overprediction of anisotropy) for station (back azimuth) averaged estimates.

4. Results

[17] We evaluate the models in terms of how well they reproduce the observed SKS splitting orientations for the Alboran region (Figure 1b) as described above. First, we

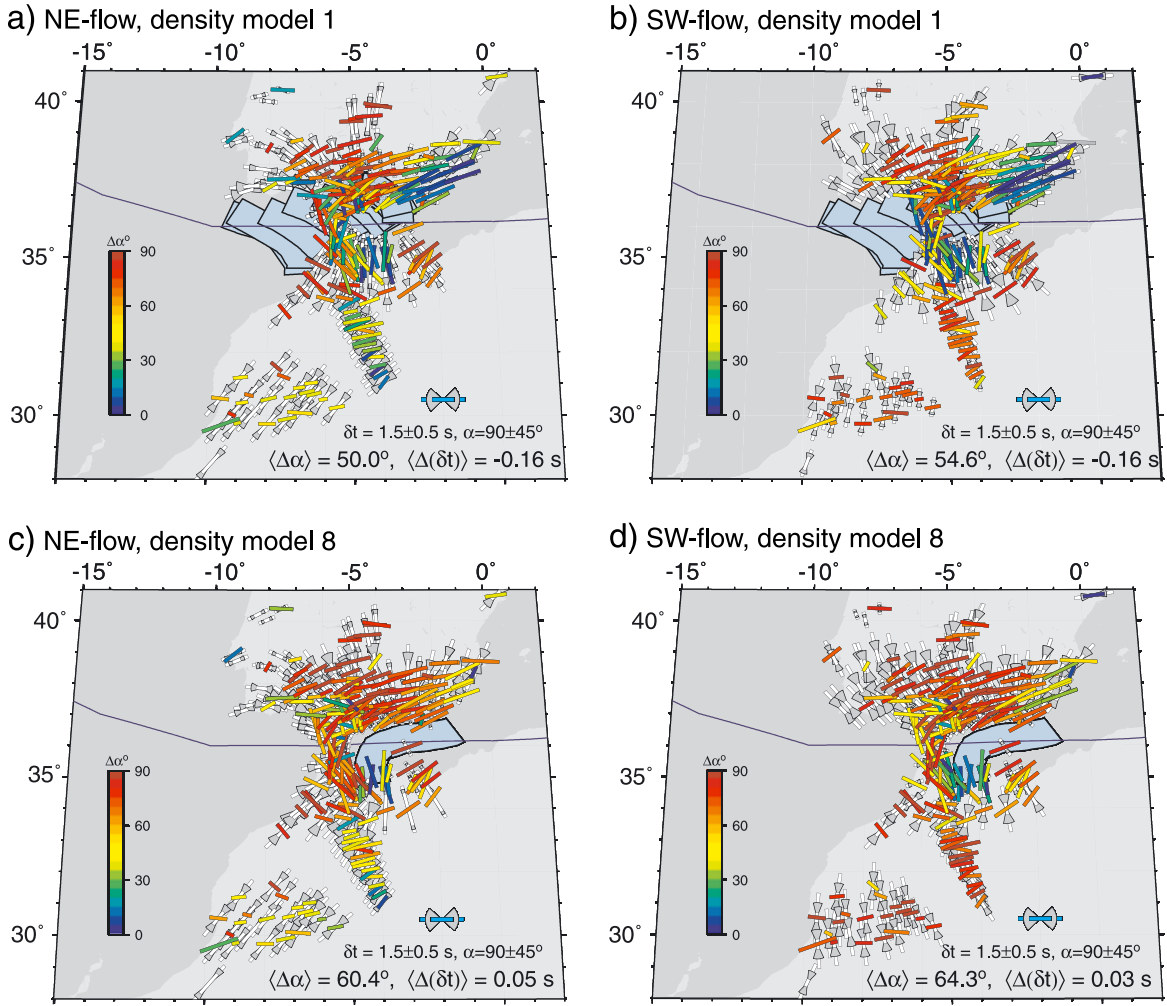


Figure 5. Examples for the effect of density structure. Model performance is shown for the (a, b) reference model plus density model 1 and (c, d) density model 8 (the best performing density model) for NE (Figures 5a and 5c) and SW flow (Figures 5b and 5d) models, with $\eta_{\text{lith}} = 50$ and a weak slab at $\eta_{\text{slab}} = 1$. Cyan contours denote the density anomalies (cf. Figure 2). See Figure 4 for legend. Note fast axes rotation for NE flow models occurs east of Gibraltar and propagates northeast while fast axes rotation occurs within the Alboran and propagates southwest for SW flow models.

discuss the general trends in modeled splitting orientations for the reference model (no additional density in the Alboran region) in terms of different mantle shear, lithosphere and slab strength, as well as stiff continental keels. We then discuss the same trends for the additional density models and provide an overview of all models examined. Lastly, we discuss our preferred model (model 8) and the implications of this mantle structure. An overview of regional misfits for four main region shown in Figure 1a is provided in Table 2.

4.1. Reference Model Results as a Function of Boundary Conditions

[18] Surface boundary conditions dominate the shallow deformation and resulting LPO formation for shallow layers ($\lesssim 150$ km), and so the surface plate motion orientation and the degree of associated shear due to net rotations have significant impacts on the resulting fast axes [Becker, 2008; Conrad and Behn, 2010]. Our reference density model for the entire Mediterranean includes the Calabrian slab

(extending to 350 km in RUM) and the more shallow Hellenic slab (≤ 200 km) with no additional structure beneath the western Mediterranean region.

[19] Without lateral viscosity variations, the fast axes orientation in the region is controlled by the surface boundary conditions, the radial viscosity structure, and hence the resulting mantle shear (Figures 3a and 3b). In the reference model, NE flow models with surface velocities >2 cm/yr in the Alboran region decrease with depth but maintain a NE orientation throughout the lithosphere. Below 100 km, horizontal velocities are slightly rotated to the NE in Spain. The resultant fast axes are oriented NE in Morocco and ENE in southern Spain (Figure 4). For SW flow models, surface velocities near the Alboran region are slower and have an E-W component along northern Morocco and a SW component in southern Spain, converging within the Alboran Sea. The sublithospheric horizontal velocities increase and rotate southward by sublithospheric shear induced by the net rotation boundary condition. The resultant fast axes are oriented nearly E-W in Spain and NNE in Morocco.

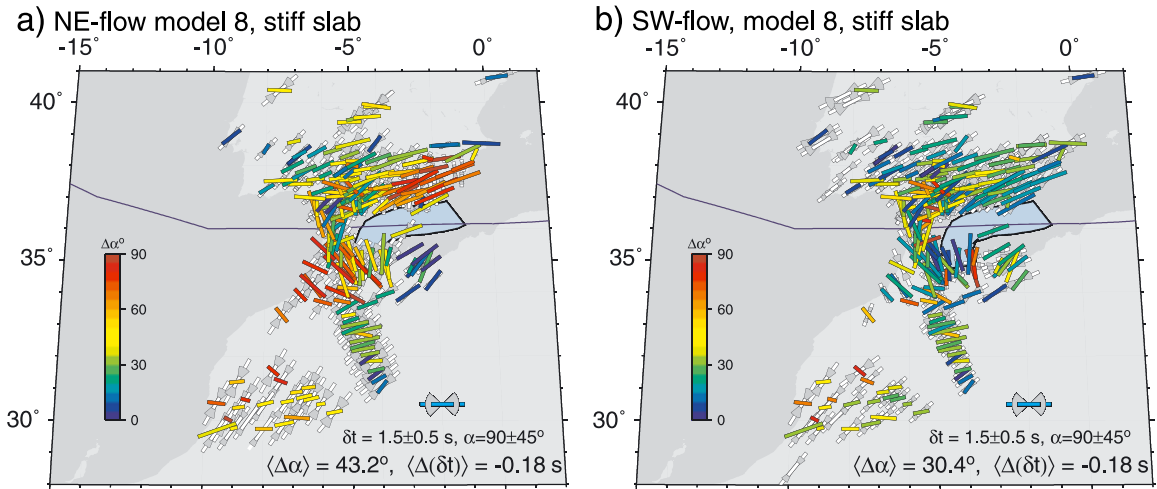


Figure 6. Effect of slab viscosity. Model performance for (a) NE flow and (b) SW flow models with best density structure model 8 and a strong slab with $\eta_{\text{lith}} = \eta_{\text{slab}} = 250$; compare to Figures 5c and 5d. See Figure 4 for legend. Note how fast axes show more plate motion orientation in southern Spain while maintaining enough buoyancy-driven deflection along Gibraltar to generate NNW-splitting orientations.

[20] Figure 4a shows the predicted anisotropy for models that essentially contain only plate motion related flow in the Alboran region (Figures 3a and 3b). Splitting orientations match moderately well in Spain but poorly in Morocco and along the Gibraltar Arc (Table 2). The splitting orientations shown in Figure 4b show an improvement in mean misfit along eastern Spain compared to NE flow (Figure 4a) but match poorly in the other domains. SW flow models perform better overall in terms of delay time misfit, particularly in western Spain and the Atlas, where the NE flow models overpredict anisotropy (Table 2).

4.2. Additional Density Beneath the Alboran Sea

[21] Twenty-one additional buoyancy structures were tested beyond the reference model (Figure 2 and section 3.1.2). Overall, we found that additional buoyancy structures beneath the Alboran Sea produce radial flow patterns as the sublithospheric flow is pulled symmetrically toward the negatively buoyant downwelling (Figure 5). Generally, flow is pulled southward across Spain and northward across the Atlas Mountains. For NE flow models, the predominant NE fast axes are reoriented to the SE in southern Spain and to the north in Morocco. For SW flow models, the SW fast axes in Spain change to a N-S orientation and the WSW fast axes in Morocco rotate to the WNW. The axis orientation depends on the morphology and location of the anomaly, and Figure 5 exemplifies this using density model 1 and model 8 (Figures 3c and 3d), which is the best performing structure. Here, we see the effect on the surface flow as it responds to the dense anomaly. Fast axes maintain plate motion orientations until proximity with the anomaly. For NE flow models, this occurs within the Alboran Sea and propagates northeastward and fast axes near Gibraltar and northern Africa are unaffected (Figures 5a and 5c, compare to Figure 4a). For SW flow models, the effect of the anomaly is strongest in the western Alboran Sea and to the southwest (Figures 5b and 5d, compare to Figure 4, and see Table 2), and fast axes in southern Spain are modified from plate motion orientations depending on the northeast extent of the anomaly.

4.3. Effects of Lateral Viscosity Variations on Additional Density Models

[22] When the viscosity of the slab is increased, the orientation of mantle flow changes from deflection toward the dense anomaly in the case of a weak slab, to deflection away from the dense anomaly for the model with a strong slab (Figures 3c, 3d, and 6). The stronger slab effectively stirs the mantle and deflects the flow more strongly. This can be interpreted in terms of changing the balance between toroidal and poloidal flow as a function of the slab viscosity [Piomallo *et al.*, 2006].

[23] Nearly all models with density anomalies perform better when the slab and lithosphere viscosities are increased, with minimum misfit values achieved at slab and lithosphere viscosities of $\sim 250\eta_0$. Increasing the slab viscosity decreases radial flow, which is a result of the downwelling, and orients the fast axes to a NE orientation for NE flow models. For the SW flow models, the fast axes rotate toward the NE in Spain and the Atlas and northward along Gibraltar, considerably improving the mean misfit (Figure 6b, Table 2). The northward deflection of flow in the SW flow models generates the NNW-splitting orientations along Gibraltar which are not generated by NE flow models with structure beneath the Alboran Sea.

[24] As suggested by Fouch *et al.* [2000] and Miller and Becker [2012], for example, the addition of a stiff continental keel dramatically affects the flow and resulting seismic anisotropy observations in a slab-continent system. Following their work, we also investigate the addition of a stiff continental keel ($100\eta_0$) that extends to 300 km beneath northwestern Africa as defined by the cratonic locations of the 3SMAC model by Nataf and Ricard [1996]. We add this cratonic keel to the strong slab model with the best density structure of Figure 6, which deflects the flow northward, increasing the magnitude of the sublithospheric flow for the NE flow models where flow is oblique to the keel margin (Figure 7a). In these models, fast axes rotate from NNE to NE in Spain, reducing the mean misfit (Table 2). Along the northern coast of Morocco, however, the fast axes

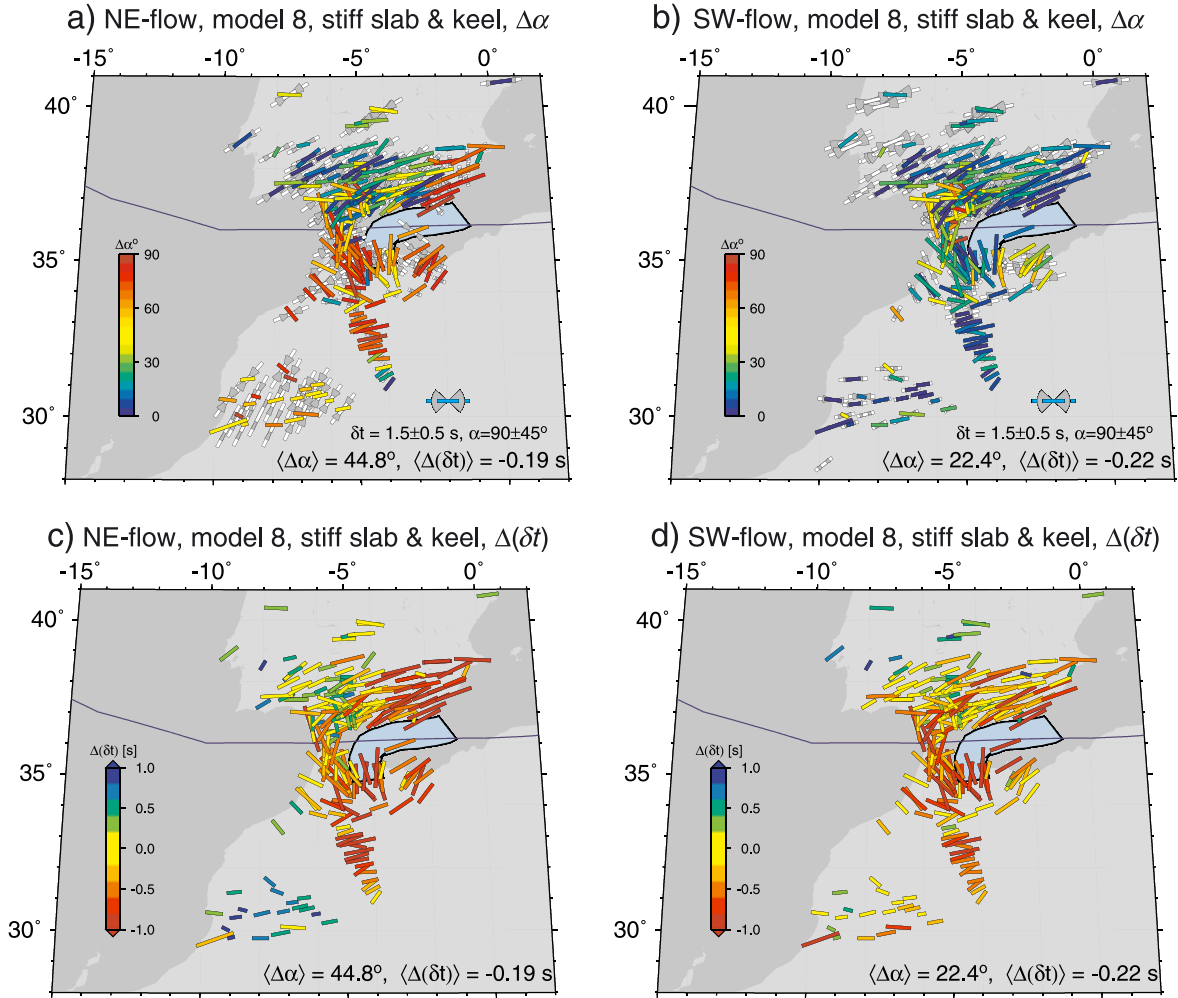


Figure 7. Predicted splitting for (a) NE flow and (b) SW flow models with model 8 as additional density, $\eta_{\text{lith}} = \eta_{\text{slab}} = 250$, and a stiff keel ($\eta_{\text{keel}} = 100$). Compare to Figures 6a and 6b, and see caption for Figure 4 for a detailed explanation. (c, d) Subplots are for the same models as in Figures 7a and 7b but have the observed splitting colored by the delay time misfit between predictions and observations (blue: overprediction and red: underprediction of anisotropy) rather than angular misfit as shown in Figures 7a and 7b.

orientations rotate NW, significantly increasing the mean misfit (Figure 7a, compared to Figure 6a). This reduces the delay time misfit along the Atlas for the NE flow keel models. For the SW flow models, flow is oriented nearly perpendicular to the keel and both mean and delay time misfits improve across the Atlas by the reduced south-directed shear in this region (Figure 7b, compared to Figure 6b, and see Table 2).

[25] Figures 7c and 7d show the same models as in Figures 7a and 7b, respectively, but colored with delay time, rather than angular, misfit. While the delay times are sensitive to modeling choices such as LPO saturation and lateral viscosity variations [Becker *et al.*, 2006b; Miller and Becker, 2012], there is a regional signal in that anisotropy strength is, on the one hand, typically underpredicted in the Alboran domain, close to the inferred slab-like sinker. On the other hand, delay times in the Atlas mountains, for example, are overpredicted, consistent with an overprinting of an

asthenospheric flow signature by frozen-in anisotropy in the lithosphere, as suggested by Miller *et al.* [2013].

4.4. Effect of Slab Gaps, Drips, and Detachment Features

[26] All density and viscosity models explored are then compared in terms of their average angular misfit with the shear wave splitting dataset in Figure 8. For several models, the density structure was modified at depth to reflect a slab gap (model 2), a drip (model 6), or slabs completely detached from the lithosphere (models 4 and 5). We find that overall mean misfit decreases significantly with the addition of a slab gap only for buoyancy-only models without the effect of plate shear. Introducing a slab gap reduces the pull from the negatively buoyant downwelling near the location of the gap. For model 6, a small drip-like structure that narrows from ~ 200 km wide at the surface to ~ 50 km wide at 400 km depth (Figure 2) is tested. This

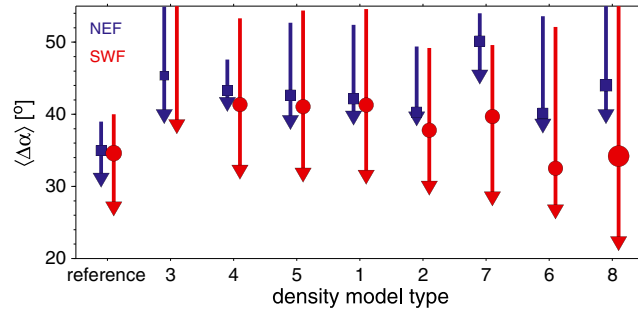


Figure 8. Average angular misfit versus density model (cf. Figure 2), where the reference is the RUM-only model, for different types of mantle shear (northeast (NE flow) and southwest (SW flow), cf. Figure 4), as defined in the text. NE flow is no-net rotation reference frame and SW flow uses a HS3 reference frame. Circles and squares (scaled by total model number) indicate the median model performance and inverted triangles mark the best model of each density type. Lines denote the range of model performance that was covered by our variations of lithospheric, slab, and keel strength, as well as modified density structures.

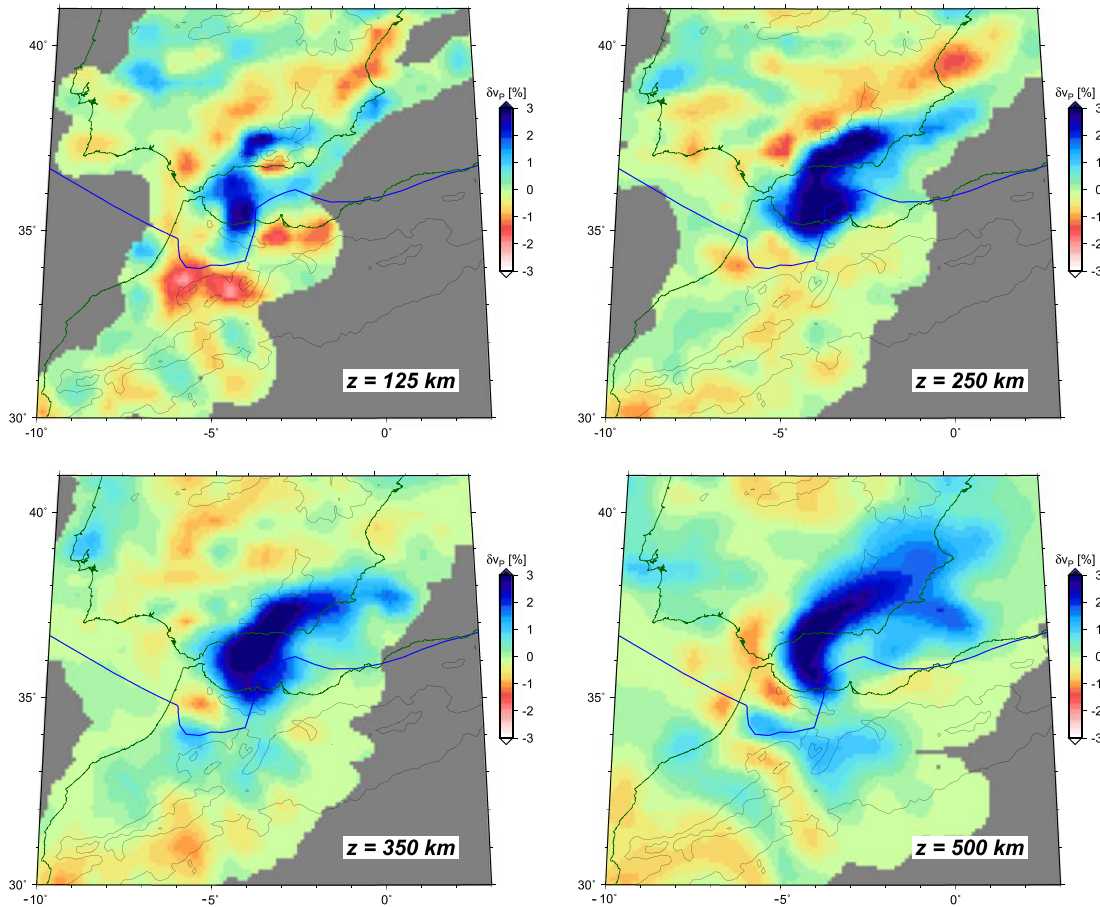


Figure 9. Regional P wave tomography obtained as part of the PICASSO project after the completion of our geodynamic modeling [Bezada *et al.*, 2013]. The structure resolved beneath the lithosphere is similar in morphology and depth extent to our independently derived, preferred density model 8 (cf. Figures 2 and 7b).

model allows for examination of the sensitivity of the predictions with the size of the anomaly. The presence of even this localized anomaly generates strong radial splitting orientations from the rotation of sublithospheric flow toward the anomaly for the buoyancy-only models. Models 4 and 5 are slab models that are completely detached from the lithosphere, extending from 300 km and 150 km, respectively, to 650 km. Yet results for model 5 are insignificantly different from those for model 1, with a continuous slab, suggesting that the splitting orientation predictions are insensitive to such a narrow detachment feature. For model 4, the results are similar to models with a slab gap, with a decrease in radial flow for the buoyancy-only models in the depth regions where the slab is detached. Where the slab is present, the flow rotates toward the anomaly, generating localized shear focused over the Granada region for the NE flow models and the Gibraltar region for the SW flow models.

[27] In summary, slabs with gaps or detached slabs do not produce significant improvements over the continuous, attached slab models tested here in terms of fitting the seismic anisotropy observations in the western Mediterranean, though the general sensitivity of our results to lateral density and viscosity variations suggests that further modifications could be considered. We infer from these results that a continuous slab that extends into the transition zone produces the best fit to the seismic anisotropy observations, compared to smaller-scale delamination or convective removal processes in the Alboran region.

4.5. Preferred Structure Beneath the Alboran Sea

[28] With the overall performance of model 8, our preferred density structure beneath the Alboran Sea includes an elongated slab beneath the Iberian margin and curving southward towards Gibraltar. This model produces the lowest overall mean misfit of 30° for a stiff slab (Figure 6b) and the SW flow type of mantle shear. Including a stiff keel based on the 3SMAC model of *Nataf and Ricard* [1996] allows for a further reduction in mean misfit (22° , Figure 7b) and improvement in the delay times match across the Atlas. When the depth extent and dip direction in model 8 is modified, while retaining the well-performing viscosity structure ($\eta_{\text{lith}} = \eta_{\text{slab}} = 250$), position of the craton, and SW flow boundary conditions, there is little improvement in overall model performance (Figure 7b). Angular misfits of $\sim 20^\circ$ are close to the best regional quantitative model misfits reported in other similar studies [e.g., *Becker et al.*, 2006b; *Miller and Becker*, 2012] and of the same order as typical uncertainties in shear wave splitting measurements [e.g., *Wüstefeld et al.*, 2009].

[29] A new P wave tomography model obtained by *Bezada et al.* [2013], which was derived independent from, and after the completion of, our geodynamic modeling, provides support for our preferred density structure. Figure 9 shows different depth maps of this tomography model, which indicate an arcuate, near-vertical subducting slab at depth [cf. *Spakman and Wortel*, 2004]. The resolved structure elongates along the Iberian margin, curving to the south and southwest around Gibraltar. These results suggest a structure beneath the Alboran Sea with a morphology and depth extent consistent with our preferred density model 8 (Figures 2 and 7b). Such a match also highlights the

capabilities of quantitative anisotropy modeling combined with a geodynamic “inverse approach” for detecting what are presumably active mantle flow components.

5. Discussion

[30] The Alboran domain is geologically complex and many of the suggested tectonic scenarios [e.g., *Platt et al.*, 2013] may be reflected in highly heterogeneous uppermost mantle structure that is not easily captured by our global flow modeling approach. In particular, within a subduction zone mantle wedge, several mechanisms other than “A” type LPO formation under present-day asthenospheric flow may be important for seismic anisotropy (e.g., reviews in *karato et al.* [2008] and *Long and Becker* [2010]). Such complications may explain some of the local mismatch between our geodynamic model predictions and the measured SKS splitting. However, our flow models are sensitive to the larger-scale patterns of anisotropy, and our best models are able to fit those patterns well. Here, we therefore focus on the dynamic effects that contribute to those regional best fit models.

5.1. Reference Frames and Net Rotation

[31] Our results highlight the importance of the absolute reference frame choice and the corresponding differences in mantle shear in our numerical models [*Becker*, 2008; *Kreemer*, 2009; *Conrad and Behn*, 2010]. SW flow models as associated with the large net rotation (HS3) kinematic boundary conditions generate a NW shear and NNW-splitting orientations along Gibraltar when combined with an imposed density anomaly beneath the Alboran Sea [cf. *Dogliani et al.*, 2007]. However, the magnitude of the net rotation (NR) in our SW flow models is inconsistent with the finding that only net rotations of $\lesssim 50\%$ of HS3 are permitted by global seismic anisotropy modeling [*Becker*, 2008; *Conrad and Behn*, 2010]. For model 8, we test variations on the magnitude of the NR component and find that mean misfit decreases with increasing NR and that models with 100% of HS3 performed best. Without the SW flow, the density models cannot generate N-S shear in response to a density anomaly beneath the Alboran region (Figure 8). We interpret this to mean that the type of SW flow that is incorporated in the best performing models is due to a component of mantle circulation not included in our flow models, and not that HS3 is the appropriate reference frame for the region. The origin of the missing component is unclear but could perhaps be related to an active upwelling or keel-deflected plume source, akin to what was suggested by *Anguita and Hernán* [2000] and *Duggen et al.* [2009].

5.2. Buoyancy and Viscosity

[32] As the chosen slab density contrast of $\sim 4\%$ is on the higher end of estimated densities, we also test several models with a density contrast of $\sim 2\%$ with a decreased match to the seismic observations in comparison to the other models. We find that for the buoyancy-only models, mean misfit differences are either insignificant or slightly improved. When the density contrast is reduced in our preferred model, the mean misfit is significantly increased due to the poor match of the splitting orientations around Gibraltar and the Atlas. Reduction of the density contrast reduces the deflection of flow around the stiff slab, reducing the N-S shear and the rotation

of splitting orientations to the NNW around Gibraltar and E-W in the Atlas.

[33] Figure 6 shows the strong effect of slab viscosity on the deflection of flow toward the buoyant anomaly. This effect is seen even for viscosity contrasts of $\eta_{\text{slab}} = 50$. We evaluate models with a constant lithosphere viscosity of $\eta_{\text{lith}} = 100$ while varying the slab viscosity among 1, 50, and $250\eta_0$. Again, these results show similar patterns with increasing slab viscosity. Further tests with slab viscosities of 5, 10, 25, and $40\eta_0$ with $\eta_{\text{lith}} = 50$ show that a slab viscosity of $25\eta_0$ is sufficient to produce a sharp decrease in vertical velocities.

5.3. Lithospheric Anisotropy

[34] In regions of fast variations of plate velocities laterally and with depth, strong LPO due to shearing may form parallel to plate motions [e.g., Long and Becker, 2010]. However, with slower relative plate velocities such as in the Alboran region, sublithospheric flow and upper mantle, small-scale convection may play a more important role. Also, within the continents, frozen-in anisotropy from past deformational cycles may have a stronger effect at lithospheric depths. In order to investigate the sensitivity of our models to these factors, we calculate mean misfit while excluding the first 100 km from our calculations. We found the best performing density structure remains to be model 8, with the same boundary conditions and viscosity structure as our preferred model. Because our preferred model produces the best match to the complex patterns along Gibraltar, it also produces the best overall mean misfit. This suggests that lithospheric anisotropy is probably less important than the deep flow in the asthenosphere associated with lateral viscosity variations and the consequence of net rotations.

6. Conclusions

[35] Our preferred model for the density structure beneath the Alboran Sea is a 500 km wide slab, elongates along the Iberian margin, extending from Granada to the Gibraltar arc, where it curves southward towards Morocco. The slab geometry extends vertically to ~ 550 km and is ~ 250 times more viscous than the surrounding mantle, providing a balance between radial flow induced by a negatively buoyant downwelling and toroidal flow induced by high viscosity. In this preferred model, initial southwest surface flow generates splitting orientations consistent with observations along Gibraltar that cannot be generated with initial northeast surface flow models. In addition, westward slab rollback need not be invoked to generate such orientations. The addition of a stiff continental keel beneath northwestern Africa improves the fit to seismic anisotropy observations with reduced delay times across the Atlas mountains by generating northward shear. Our preferred density structure is consistent with new structural seismology imaging, derived independently from our work. This highlights the potential of geodynamic inverse modeling of seismic anisotropy for regional tectonic studies.

[36] **Acknowledgments.** This study was supported by the National Science Foundation, Continental Dynamics (EAR-0809023), and CAREER (EAR-1054638). Computations were conducted at the University of Southern California Center for High Performance Computing and Communications (www.usc.edu/hpcc). A special thanks to IRIS PASSCAL, C.P. Ryan, M. Harnafi, D. Elouai, and all the people at L'Institut Scientifique at

Mohammad V University in Rabat and our collaborators at ICTJA-CSIC who made the seismic experiment possible. We thank seismologists sharing their models in electronic form, J. Wookey, J. Platt, J. Diaz, and E. Humphreys for comments on an early draft, three reviewers for helpful suggestions, and CitcomS code contributors, including S. Zhong, E. Tan, A. McNamara, and L. Moresi and CIG, for their efforts in sharing and maintaining this software. All figures were produced with Generic Mapping Tools [Wessel and Smith, 1991].

References

- Alpert, L. A., T. W. Becker, and I. W. Bailey (2010), Global slab deformation and centroid moment constraints on viscosity, *Geochem. Geophys. Geosyst.*, *11*, Q12006, doi:10.1029/2010GC003301.
- Anguita, F., and F. Hernán (2000), The Canary Islands origin: A unifying model, *J. Volcanol. Geotherm. Res.*, *103*, 1–26.
- Becker, T. W. (2006), On the effect of temperature and strain-rate dependent viscosity on global mantle flow, net rotation, and plate-driving forces, *Geophys. J. Int.*, *167*, 943–957.
- Becker, T. W. (2008), Azimuthal seismic anisotropy constrains net rotation of the lithosphere, *Geophys. Res. Lett.*, *35*, L08308, doi:10.1029/2008GL033946.
- Becker, T. W., and C. Faccenna (2011), Mantle conveyor beneath the Tethyan collisional belt, *Earth Planet. Sci. Lett.*, *310*, 453–461.
- Becker, T. W., J. B. Kellogg, G. Ekström, and R. J. O'Connell (2003), Comparison of azimuthal seismic anisotropy from surface waves and finite-strain from global mantle-circulation models, *Geophys. J. Int.*, *155*, 696–714.
- Becker, T. W., S. Chevrot, V. Schulte-Pelkum, and D. K. Blackman (2006a), Statistical properties of seismic anisotropy predicted by upper mantle geodynamic models, *J. Geophys. Res.*, *111*, B08309, doi:10.1029/2005JB004095.
- Becker, T. W., V. Schulte-Pelkum, D. K. Blackman, J. B. Kellogg, and R. J. O'Connell (2006b), Mantle flow under the western United States from shear wave splitting, *Earth Planet. Sci. Lett.*, *247*, 235–251.
- Becker, T. W., B. Kustowski, and G. Ekström (2008), Radial seismic anisotropy as a constraint for upper mantle rheology, *Earth Planet. Sci. Lett.*, *267*, 213–237.
- Behn, M. D., C. P. Conrad, and P. G. Silver (2004), Detection of upper mantle flow associated with the African Superplume, *Earth Planet. Sci. Lett.*, *224*, 259–274.
- Ben Ismail, W., and D. Mainprice (1998), An olivine fabric database: An overview of upper mantle fabrics and seismic anisotropy, *Tectonophysics*, *296*, 145–157.
- Bezada, M. J., and E. D. Humphreys (2012), Contrasting rupture processes during the April 11, 2010 deep-focus earthquake beneath Granada, Spain, *Earth Planet. Sci. Lett.*, *353*, 38–46.
- Bezada, M. J., E. D. Humphreys, D. R. Toomey, M. Harnafi, J. M. Dávila, and J. Gallart (2013), Evidence for slab rollback in westernmost Mediterranean from improved upper mantle imaging, *Earth Planet. Sci. Lett.*, *368*, 51–60.
- Bijwaard, H., W. Spakman, and E. Engdahl (1998), Closing the gap between regional and global travel time tomography, *J. Geophys. Res.*, *103*, 30,055–30,078.
- Bird, P. (2003), An updated digital model of plate boundaries, *Geochem. Geophys. Geosyst.*, *4*(3), 1027, doi:10.1029/2001GC000252.
- Blackman, D. K., and J.-M. Kendall (2002), Seismic anisotropy of the upper mantle: 2. Predictions for current plate boundary flow models, *Geochem. Geophys. Geosyst.*, *3*(9), 8602, doi:10.1029/2001GC000247.
- Blanco, M., and W. Spakman (1993), The P-wave velocity structure of the mantle below the Iberian Peninsula: Evidence for subducted lithosphere below southern Spain, *Tectonophysics*, *221*, 13–34.
- Bokelmann, G., and E. Mauffro (2007), Mantle structure under Gibraltar constrained by dispersion of body waves, *Geophys. Res. Lett.*, *34*, L22305, doi:10.1029/2007GL030964.
- Bowman, J. R., and M. A. Ando (1987), Shear-wave splitting in the upper mantle wedge above the Tonga subduction zone, *Geophys. J. R. Astron. Soc.*, *88*, 24–41.
- Buforn, E., C. Pro, A. Udias, and C. del Fresno (2011), The 2010 Granada, Spain deep earthquake, *Bull. Seismol. Soc. Am.*, *101*, 2418–2430.
- Buontempo, L., G. H. R. Bokelmann, G. Barruol, and J. Morales (2008), Seismic anisotropy beneath southern Iberia from SKS splitting, *Earth Planet. Sci. Lett.*, *273*, 237–250.
- Conrad, C. P., and M. Behn (2010), Constraints on lithosphere net rotation and asthenospheric viscosity from global mantle flow models and seismic anisotropy, *Geochem. Geophys. Geosyst.*, *11*, Q05W05, doi:10.1029/2009GC002970.

- DeMets, C., R. G. Gordon, D. F. Argus, and S. Stein (1994), Effect of recent revisions to the geomagnetic reversal time scale on estimates of current plate motions, *Geophys. Res. Lett.*, *21*, 2191–2194.
- Diaz, J., J. Gallart, A. Villaseñor, F. Mancilla, A. Pazos, D. Córdoba, J. A. Pulgar, P. Ibarra, and M. Harnafi (2010), Mantle dynamics beneath the Gibraltar Arc (western Mediterranean) from shear-wave splitting measurements on a dense seismic array, *Geophys. Res. Lett.*, *37*, L18304, doi:10.1029/2010GL044201.
- Doglioni, C., E. Carminati, M. Cuffaro, and D. Scrocca (2007), Subduction kinematics and dynamic constraints, *Earth Sci. Rev.*, *83*, 125–175.
- Duggen, S., K. Hoernle, F. Hauff, A. Klügel, M. Bouabdellah, and M. F. Thirlwall (2009), Flow of Canary mantle plume material through a sub-continental lithospheric corridor beneath Africa to the Mediterranean, *Geology*, *37*, 283–286.
- Engdahl, E. R., R. D. van der Hilst, and R. Buland (1998), Global teleseismic earthquake relocation with improved travel times and procedures for depth determination, *Bull. Seismol. Soc. Am.*, *88*, 722–743.
- Faccenna, C., and T. W. Becker (2010), Shaping mobile belts by small-scale convection, *Nature*, *465*, 602–605.
- Faccenna, C., C. Piromallo, A. Crespo Blanc, L. Jolivet, and F. Rossetti (2004), Lateral slab deformation and the origin of the arcs of the western Mediterranean, *Tectonics*, *23*, TC1012, doi:10.1029/2002TC001488.
- Fischer, K. M., and D. A. Wiens (1996), The depth distribution of mantle anisotropy beneath the Tonga subduction zone, *Earth Planet. Sci. Lett.*, *142*, 253–260.
- Fouch, M. J., K. M. Fischer, E. M. Parmentier, M. E. Wysession, and T. J. Clarke (2000), Shear wave splitting, continental keels, and patterns of mantle flow, *J. Geophys. Res.*, *105*, 6255–6275.
- Gaboret, C., A. M. Forte, and J.-P. Montagner (2003), The unique dynamics of the Pacific Hemisphere mantle and its signature on seismic anisotropy, *Earth Planet. Sci. Lett.*, *208*, 219–233.
- Gripp, A. E., and R. G. Gordon (2002), Young tracks of hotspots and current plate velocities, *Geophys. J. Int.*, *150*, 321–361.
- Gudmundsson, O., and M. Sambridge (1998), A regionalized upper mantle (RUM) seismic model, *J. Geophys. Res.*, *103*, 7121–7136.
- Gutscher, M.-A., J. Malod, J.-P. Rehault, I. Contrucci, F. Klingelhofer, L. Mendes-Victor, and W. Spakman (2002), Evidence for active subduction beneath Gibraltar, *Geology*, *30*, 1071–1074.
- Gutscher, M.-A., et al. (2012), The Gibraltar subduction: A decade of new geophysical data, *Tectonophysics*, *574*, 72–91.
- Hall, C. E., K. M. Fischer, E. M. Parmentier, and D. K. Blackman (2000), The influence of plate motions on three-dimensional back arc mantle flow and shear wave splitting, *J. Geophys. Res.*, *105*, 28,009–28,033.
- Jiménez-Munt, I., M. Fernández, J. Vergés, D. García-Castellanos, J. Fullea, M. Pérez-Gussinyé, and J. C. Afonso (2011), Decoupled crust-mantle accommodation of Africa-Eurasia convergence in the NW Moroccan margin, *J. Geophys. Res.*, *116*, B08403, doi:10.1029/2010JB008105.
- Jolivet, L., C. Faccenna, and C. Piromallo (2009), From mantle to crust: Stretching the Mediterranean, *Earth Planet. Sci. Lett.*, *285*, 198–209.
- Kaminski, É., and N. M. Ribe (2001), A kinematic model for for recrystallization and texture development in olivine polycrystals, *Earth Planet. Sci. Lett.*, *189*, 253–267.
- Kaminski, É., N. M. Ribe, and J. T. Browaeys (2004), D-Rex, a program for calculation of seismic anisotropy due to crystal lattice preferred orientation in the convective upper mantle, *Geophys. J. Int.*, *157*, 1–9.
- Karato, S.-i. (1992), On the Lehmann discontinuity, *Geophys. Res. Lett.*, *51*, 2255–2258.
- Karato, S.-i., H. Jung, I. Katayama, and P. Skemer (2008), Geodynamic significance of seismic anisotropy of the upper mantle: New insights from laboratory studies, *Annu. Rev. Earth Planet. Sci.*, *36*, 59–95.
- Koulali, A., et al. (2011), New GPS constraints on active deformation along the Africa-Iberia plate boundary, *Earth Planet. Sci. Lett.*, *308*, 211–217.
- Kreemer, C. (2009), Absolute plate motions constrained by shear wave splitting orientations with implications for hot spot motions and mantle flow, *J. Geophys. Res.*, *114*, B10405, doi:10.1029/2009JB006416.
- Li, C., R. D. van der Hilst, E. R. Engdahl, and S. Burdick (2008), A new global model for P wave speed variations in Earth's mantle, *Geochem. Geophys. Geosyst.*, *9*, Q05018, doi:10.1029/2007GC001806.
- Lonergan, L., and N. White (1997), Origin of the Betic-Rif mountain belt, *Tectonics*, *16*, 504–522.
- Long, M. D., and T. W. Becker (2010), Mantle dynamics and seismic anisotropy, *Earth Planet. Sci. Lett.*, *297*, 341–354.
- Miller, M. S., and T. W. Becker (2012), Mantle flow deflected by interactions between subducted slabs and cratonic keels, *Nat. Geosci.*, *5*, 726–730.
- Miller, M. S., L. A. Alpert, A. Allam, and T. W. Becker (2012), Mantle dynamics and structure beneath the Western Mediterranean constrained by seismic anisotropy and global flow models, *13th Symposium of SEDI*, Leeds, UK.
- Miller, M. S., A. Allam, T. W. Becker, J. F. DiLeo, and J. Wookey (2013), Constraints on the geodynamic evolution of the westernmost Mediterranean and northwestern Africa from shear wave splitting analysis, *Earth Planet. Sci. Lett.*, *375*, 234–243, doi:10.1016/j.epsl.2013.05.036.
- Moresi, L. N., and M. Gurnis (1996), Constraints on the lateral strength of slabs from three-dimensional dynamic flow models, *Earth Planet. Sci. Lett.*, *138*, 15–28.
- Nataf, H.-C., and Y. Ricard (1996), 3SMAC: An *a priori* tomographic model of the upper mantle based on geophysical modeling, *Phys. Earth Planet. Inter.*, *95*, 101–122.
- Pedrerà, A., et al. (2011), Is there an active subduction beneath the Gibraltar orogenic arc? Constraints from Pliocene to present-day stress field, *J. Geodyn.*, *52*, 83–96.
- Piromallo, P., T. W. Becker, F. Funiciello, and C. Faccenna (2006), Three-dimensional instantaneous mantle flow induced by subduction, *Geophys. Res. Lett.*, *33*, L08304, doi:10.1029/2005GL025390.
- Platt, J. P., and R. L. M. Vissers (1989), Extensional collapse of thickened continental lithosphere: A working hypothesis for the Alboran Sea and Gibraltar arcs, *Geology*, *17*, 540–543.
- Platt, J. P., W. M. Behr, K. Johannesen, and J. R. Williams (2013), The Betic-Rif Arc and its orogenic hinterland: A review, *Annu. Rev. Earth Planet. Sci.*, *41*, 1–14.
- Royden, L. H. (1993), Evolution of retreating subduction boundaries formed during continental collision, *Tectonics*, *12*, 629–638.
- Savage, M. K. (1999), Seismic anisotropy and mantle deformation: What have we learned from shear wave splitting? *Rev. Geophys.*, *37*, 65–106.
- Seber, D., M. Barazangi, A. Ibenbrahim, and A. Demnati (1996), Geophysical evidence for lithospheric delamination beneath the Alboran Sea and Rif-Betic mountains, *Nature*, *379*, 785–790.
- Silver, P. G. (1996), Seismic anisotropy beneath the continents: Probing the depths of geology, *Annu. Rev. Earth Planet. Sci.*, *24*, 385–432.
- Spakman, W., and R. Wortel (2004), A tomographic view on western Mediterranean geodynamics, in *The TRANSMED Atlas. The Mediterranean Region from Crust to Mantle*, edited by W. Cavazza et al., pp. 31–52, Springer, Berlin, Germany.
- Tanimoto, T., and D. L. Anderson (1984), Mapping convection in the mantle, *Geophys. Res. Lett.*, *11*, 287–290.
- Tommasi, A., D. Mainprice, G. Canova, and Y. Chastel (2000), Viscoplastic self-consistent and equilibrium-based modelling of olivine lattice preferred orientation. 1. Implications for the upper mantle seismic anisotropy, *J. Geophys. Res.*, *105*, 7893–7908.
- Vinnik, L. P., R. Kind, G. L. Kosarev, and L. Makeyeva (1989), Azimuthal anisotropy in the lithosphere from observations of long-period s-waves, *Geophys. J. Int.*, *99*, 549–559.
- Wenk, H.-R., and C. N. Tomé (1999), Modeling dynamic recrystallization of olivine aggregates deformed in simple shear, *J. Geophys. Res.*, *104*, 25,513–25,527.
- Wessel, P., and W. H. F. Smith (1991), Free software helps map and display data, *Eos Trans. AGU*, *72*, 445–446.
- Wüstefeld, A., G. Bokelmann, C. Zaroli, and G. Barruol (2008), Split-Lab: A shear-wave splitting environment in Matlab, *Comput. Geosci.*, *34*, 518–528.
- Wüstefeld, A., G. H. R. Bokelmann, G. Barruol, and J. P. Montagner (2009), Identifying global seismic anisotropy patterns by correlating shear-wave splitting and surface-wave data, *Phys. Earth Planet. Inter.*, *176*, 198–212, database available online at <http://www.gm.univ-montp2.fr/splitting/DB/>.
- Zeck, H. P. (1996), Betic-Rif orogeny: Subduction of Mesozoic Tethys lithosphere under eastward drifting Iberia, slab detachment shortly before 22 Ma, and subsequent uplift and extensional tectonics, *Tectonophysics*, *254*, 1–16.
- Zhong, S. (2001), Role of ocean-continent contrast and continental keels on plate motion, net rotation of lithosphere, and the geoid, *J. Geophys. Res.*, *106*, 703–712.
- Zhong, S., M. T. Zuber, L. Moresi, and M. Gurnis (2000), Role of temperature-dependent viscosity and surface plates in spherical shell models of mantle convection, *J. Geophys. Res.*, *105*, 11,063–11,082.